

Theoretical Evaluation and Comparison of Fast Chemical Shift Imaging Methods

R. Pohmann, M. von Kienlin, and A. Haase

Physikalisches Institut, Lehrstuhl für experimentelle Physik V, Universität Würzburg, 97074 Würzburg, Germany

Received January 30, 1997

Magnetic resonance chemical shift imaging (CSI) is becoming the method of choice for localized NMR spectroscopic examinations, allowing simultaneous detection of NMR spectra from a large number of voxels. The main limitation of these methods is their long experimental duration. A number of fast CSI experiments have been presented, promising to reduce that duration. In this contribution the criteria for evaluating and optimizing the sensitivity of fast CSI experiments are elaborated. For a typical experiment in the human brain, the performance of various methods is compared. While conventional CSI provides optimal sensitivity per unit time, it is shown in which circumstances fast sequences allow a shorter experimental duration. Using these results, the best method for any experimental requirements can be selected.

© 1997 Academic Press

Key Words: fast spectroscopic imaging; sensitivity.

INTRODUCTION

Chemical shift imaging (CSI) already is an established tool for studying *in vivo* biochemistry and metabolic pathways in fundamental biomedical research. CSI is also emerging as a valuable diagnostic instrument. NMR spectroscopy has been successfully applied to finding the seizure foci in temporal lobe epilepsy (1, 2), to studying brain metabolic alterations in patients with AIDS (3), or to detecting at a very early stage tumor response to chemotherapy (4). Preliminary studies have also shown that CSI might be valuable for investigating noninvasively abnormal cardiac energy metabolism in various pathologies (5, 6).

Probably the most serious limitation of CSI is its long experimental duration, which is dictated by two factors: First, CSI suffers from the inherently low sensitivity of NMR. As the signal-to-noise ratio (SNR) decreases with the voxel size, this factor becomes predominant with increasing spatial resolution and will impose its ultimate limit. The second factor is the number of repetitions required by the experimental protocol, i.e., the number of phase encoding steps. Irrespective of the sensitivity, the minimal duration of the experiment is determined by that number. This latter point may be dominant in examinations with three spatial (7) or with two spectral (8, 9) dimensions, where the number of required steps is high.

To cope with the long experimental duration, a number of fast CSI sequences have been developed in the past years, mostly derived from one of the fast imaging techniques. By ingeniously varying how spatial and spectral information is obtained, they attempt to reduce the experiment time and to still obtain a good SNR. As the spatial resolution will ultimately be limited by sensitivity, it is crucial that any of these fast methods exploit the available magnetization at its best.

In the present work we have established criteria for analyzing the properties of the most prominent fast CSI sequences. In the first section, the general parameters needed to compare the performance of an experiment are defined. Preparation period, excitation, and signal acquisition are treated in a modular way, giving insight into the principles of how to obtain optimal sensitivity. In the second section, these principles will be applied to analyze the behavior of 11 different CSI methods. For a typical CSI experiment which might be conducted on a clinical whole-body instrument, the performance of these techniques is compared in terms of sensitivity and minimal duration. The formulas established for the individual sequences also allow one to analyze their properties under other experimental conditions. These results will help to select the appropriate method for any application of *in vivo* CSI. By improving the quality and the information content of the experiments conducted, this should further enhance the biomedical and clinical impact of CSI.

I. THE SENSITIVITY OF A CSI EXPERIMENT

Throughout the following calculations, a given experimental setup is assumed. The sample and its properties, the RF coil (especially its sensitivity), and the whole MR instrument are always the same and determine the physical setting of the examination. To compare the sensitivity of various measurement methods performed on this setup, only the effects of the pulse sequence and its parameters need to be considered.

For the calculation of the sensitivity, each sequence is divided into four parts, which can be described separately: (a) excitation of the magnetization with RF pulses, (b) prep-

ation period used to encode the desired spectral or spatial information, (c) acquisition of the signal, followed finally by (d) a delay for relaxation. The excitation scheme and the repetition time determine the maximal amplitude of the free induction decay (FID) or spin-echo signal, $A(T_R, T_E, \alpha)$, which depends on the excitation angle α , on the repetition time T_R , and, for spin echoes, on the echo time T_E . Further parameters that influence A , such as the longitudinal and transverse relaxation times T_1 and T_2 , which depend only on sample and hardware characteristics, are supposed to be fixed and thus do not appear in the parameter lists in the parentheses. The signal is also modulated during the spin preparation period, for instance, due to the signal decay during the delay needed for phase encoding. Such effects will be described by a factor V_{prep} . The signal is then sampled and Fourier transformed, which has the effect of integrating over the FID or echo. The amplitude in the frequency domain thus is also influenced by the shape of the time domain signal; this is described by a factor $f(T_{\text{AQ}}, \Delta f)$. It depends on the bandwidth Δf used for sampling and on the acquisition time T_{AQ} . This modular approach simplifies the analytical description of the influence of the many experimental parameters involved in a CSI examination and allows one to compute the sensitivity of various methods.

Signal and Noise in the Time Domain

The first step in calculating the sensitivity of an experiment is to look at the signal and noise of the acquired data in the time domain. For the moment, we restrict ourselves to single-pulse excitation methods, where an FID is observed by applying only one excitation pulse per repetition. Spin-echo experiments will be treated in a later section.

An FID, which is sampled in discrete time intervals Δt according to the Shannon criterion $\Delta t = 1/\Delta f$ (Δf : sampling bandwidth), consists, for a single resonance, of an oscillation with frequency ν_0 and an exponential decay with time constant T_2^* ,

$$s(n\Delta t) = A \cdot e^{2\pi i\nu_0 n\Delta t} \cdot e^{-n\Delta t/T_2^*}, \quad [1]$$

where i is $\sqrt{-1}$, $s(n\Delta t)$ is the signal of the n th sampled data point at the time $n\Delta t$, and A is the amplitude of the FID immediately after the excitation pulse, $A = s(t = 0)$.

A general expression for A can be derived for a sequence of excitations with a constant repetition time T_R and excitation angle α . According to the Bloch equations, the behavior of the longitudinal magnetization M_z during T_R in the absence of RF radiation is described by

$$M_z(t) = M_z(t = 0) \cdot e^{-t/T_1} + M_0 \cdot (1 - e^{-t/T_1}), \quad [2]$$

M_0 being the magnetization of the sample in thermal equilibrium.

In the course of a great number of repetitions, the system

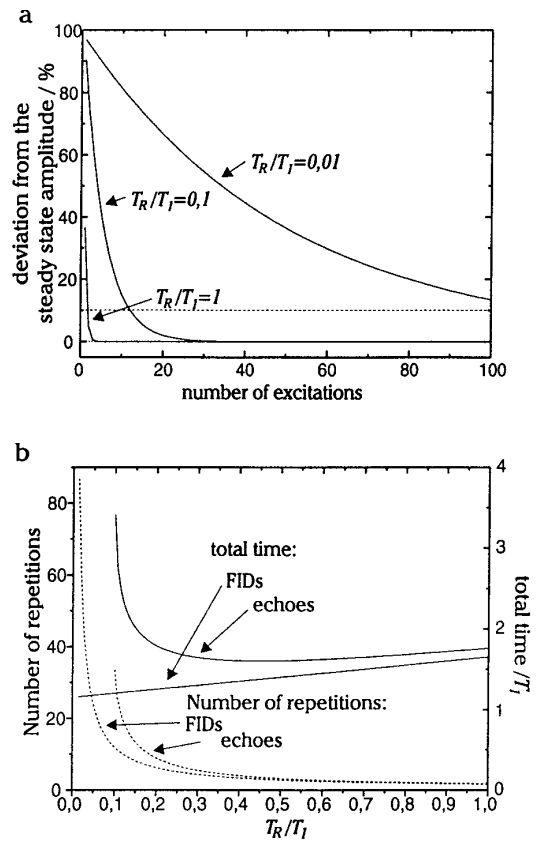


FIG. 1. (a) Behavior of the amplitude of the first 100 FIDs in an experiment consisting of equally spaced excitation pulses, using the Ernst angle. The deviation of the FID amplitude from the steady-state value is plotted for three different repetition times. The system is presumed to be in the steady state, when the amplitude is within 10% of the steady-state amplitude (broken line). (b) The number of excitations needed to reach the steady-state signal (dotted lines) is small for long repetition times. The total duration needed to reach the steady state (straight line) thus depends only weakly on T_R , but is always between $1.5T_1$ and $2T_1$ for FIDs and echoes with a repetition time greater than $0.2T_1$. For echoes, an echo time of $T_E = 0.1T_1$ is assumed.

approaches a steady state, in which the size of the longitudinal magnetization is the same for every excitation. Then, every FID has the same amplitude:

$$A_{\text{FID}}(T_R, \alpha) = M_0 \cdot \frac{1 - e^{-T_R/T_1}}{1 - \cos \alpha \cdot e^{-T_R/T_1}} \cdot \sin \alpha. \quad [3]$$

The Ernst angle, which maximizes the signal amplitude for a given T_R and T_1 , can be found by differentiating this expression by α and is $\cos \alpha_{\text{ernst}} = e^{-T_R/T_1}$ (10, 11). It is small for short repetition times and tends to 90° for $T_R \gg T_1$.

Expression [3] can be used only in the steady state, that is, if the total experiment consists of a far greater number of excitations than needed to reach a constant FID amplitude. For the case of excitation with the Ernst angle, Fig. 1a shows the course of the FID amplitude during the first 100 excita-

tions for three different repetition or relaxation times. Figure 1b displays the number of excitations and the total time needed to get within 10% of the steady-state amplitude. It can be seen that irrespective of the repetition time this always takes less than $2T_1$, which is much shorter than the usual duration of a CSI experiment. For the following calculations we can therefore assume the steady state and use Eq. [3] to describe the time domain amplitude. The time domain signal of an FID for a single resonance is then accurately described by putting Eq. [3] into [1].

To this signal a statistical noise is added, which is caused by electron fluctuations in coil and sample. Its amplitude is independent of the frequency, but does depend on the characteristics of coil and sample as well as on the bandwidth Δf of the filter that is used to avoid noise aliasing. The standard deviation of this noise is given by the Johnson noise formula (12),

$$\langle \sigma_t \rangle = \sqrt{4kT_c R \Delta f} = a \cdot \sqrt{\Delta f}, \quad [4]$$

where the brackets are used to label a statistical variable. Here, k is the Boltzmann constant, T_c is the temperature of the coil, and R contains the coil resistance as well as a characteristic resistance describing losses in the sample (13). Since all of these parameters depend only on the apparatus and the sample, which are both presumed to be constant, they can all be included in a proportionality factor a . It describes the noise per unit bandwidth and is called the spectral noise density. For a given experimental setup, a is the same for any method, since the resistance of the loaded coil seen through the matching network is usually equal to 50Ω . Of all the parameters that influence the noise amplitude, the only one that depends on the method used, and thus the only one of interest here, is the bandwidth Δf .

Signal and Noise in the Spectral Domain

In an NMR experiment the acquired data are usually transferred into the frequency domain by Fourier transformations. In order to analyze the performance of an experiment, it is therefore necessary to determine the effects of this transformation. First, we restrict ourselves to the spectral dimension. The results will then be applied to the spatial dimensions in a later section. We also postpone the discussion of postprocessing of the signal and assume first unfiltered FIDs.

The discrete Fourier transformation is defined as

$$S(\nu) = \sum_{n=0}^{N-1} e^{-2i\pi\nu n \Delta t} s(n \Delta t), \quad [5]$$

where $S(\nu)$ is the signal amplitude at the frequency ν , N is the number of points acquired with the temporal spacing ("dwell time") Δt , and $s(n \Delta t)$ is the signal of the n th point in the time domain.

The peak amplitude of a spectral line at the frequency ν_0

can be determined by putting the time domain signal, Eq. [1], into Eq. [5]:

$$\begin{aligned} S(\nu_0) &= A \cdot \sum_{n=0}^{N-1} e^{-2i\pi\nu_0 n \Delta t} e^{2i\pi\nu_0 n \Delta t} e^{-n \Delta t / T_2^*} \\ &= A \cdot \sum_{n=0}^{N-1} e^{-n \Delta t / T_2^*} \approx A \cdot \frac{1}{\Delta t} \int_0^{T_{AQ}} e^{-t/T_2^*} dt \\ &= A \cdot f(T_{AQ}, \Delta f). \end{aligned} \quad [6]$$

The conversion of the sum into an integral in this calculation is possible as long as the dwell time is much shorter than T_2^* . This condition is fulfilled in most CSI experiments.

In Eq. [6], we defined the factor $f(T_{AQ}, \Delta f)$, which describes the influence of the summation carried out in the Fourier transformation. Solving the integral in Eq. [6], this factor is found for FIDs:

$$f_{\text{FID}}(T_{AQ}, \Delta f) = T_2^* \cdot \Delta f \cdot (1 - e^{-T_{AQ}/T_2^*}). \quad [7]$$

A long FID with a long T_2^* thus generates a higher peak amplitude than a rapidly decreasing signal or one that is sampled only over a short time T_{AQ} . The bandwidth in this equation reflects that with our definition of the Fourier transformation the peak amplitude grows if a larger number of data points is sampled within a constant acquisition time.

To determine the noise amplitude in the spectral domain, we must apply the Fourier transformation to Eq. [4], where we must consider the statistical behavior of noise. In the frequency domain, the standard deviation of noise $\langle \sigma_\nu \rangle$ results as

$$\langle \sigma_\nu \rangle^2 = \sum_{n=1}^N \langle \sigma_t \rangle^2 = N \langle \sigma_t \rangle^2, \quad [8]$$

and thus, inserting Eq. [4],

$$\sigma_\nu = a \cdot \sqrt{N \cdot \Delta f}. \quad [9]$$

For an experiment with a resolution of N points, the noise amplitude in the frequency domain thus is \sqrt{N} times the noise in the FID.

A CSI experiment combines one spectral with up to three spatial dimensions, requiring as many Fourier transformations for reconstruction. For both signal and noise this must be taken into account by adding one factor of type f , Eq. [7], for every dimension in the signal and of $\sqrt{N_i}$ in the noise, N_i being the number of points in the spectral ($i = \delta$) or the respective spatial dimension ($i = x, y, z$). The factor f describing the signal amplitude of spatially resolved experiments is derived in a later section.

The Sensitivity

The SNR of a spectral line is defined as its peak height divided by the standard deviation of the noise (14). Using Eqs. [6] and [9], we get for an FID

$$\text{SNR} = \frac{A_{\text{FID}}(T_R, \alpha) \cdot f_{\text{FID}}(T_{\text{AQ}}, \Delta f)}{a \cdot \sqrt{\Delta f \cdot N}}. \quad [10]$$

A comparison of different pulse sequences also must take into account the total duration of an experiment, T_{tot} . A useful criterion thus is the sensitivity Ψ , which is defined as the SNR divided by the square root of T_{tot} :

$$\Psi = \frac{\text{SNR}}{\sqrt{T_{\text{tot}}}}. \quad [11]$$

The sensitivity of an experiment is then determined by dividing Eq. [6] by Eq. [9] and the square root of T_{tot} :

$$\Psi = \frac{A(T_R, \alpha) \cdot f(T_{\text{AQ}}, \Delta f)}{a \cdot \sqrt{\Delta f \cdot N \cdot T_{\text{tot}}}}. \quad [12]$$

This sensitivity is a measure of how efficiently the available magnetization is used, and thus is a suitable criterion for analyzing the signal-to-noise performance of an NMR experiment.

The Optimum Acquisition Parameters

The sensitivity as defined by Eq. [12] should always be optimized with respect to the experimental parameters α , T_R , and T_{AQ} . Since the optimum flip angle has already been derived, we will now look at the repetition time T_R :

In an experiment with M excitations and a constant repetition time T_R , the total experiment duration is $T_{\text{tot}} = M \cdot T_R$. Keeping only the T_R -dependent terms of Eq. [12] yields the total accumulated magnetization per unit time that is detected in the experiment (14):

$$M_{\text{tot}} = \frac{A(T_R)}{\sqrt{T_R}}. \quad [13]$$

We assume the Ernst angle to be used for excitation. Then α is determined by T_R and T_1 and is no longer an independent parameter of A . The dependence of this expression on the repetition time is plotted in Fig. 2. It can be seen that it has a maximum for very short repetition times. The highest accumulated magnetization would for FIDs therefore be obtained by keeping the repetition time as short as possible.

To optimize the acquisition time T_{AQ} , we examine the T_{AQ} -dependent terms of Eq. [12] that constitute the SNR of a single FID,

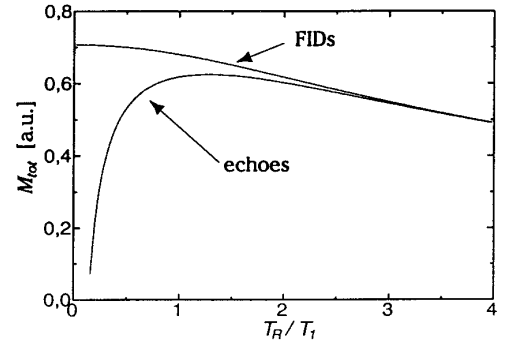


FIG. 2. Dependence of the total accumulated magnetization, Eq. [13], on the repetition time for FIDs and echoes with an echo time of $0.15T_1$ and $T_2 = \infty$.

$$\text{SNR} = \frac{T_2^* \cdot (1 - e^{-T_{\text{AQ}}/T_2^*})}{a \cdot \sqrt{T_{\text{AQ}}}}, \quad [14]$$

where we used the fact that the Shannon theorem implies that $T_{\text{AQ}} = N\Delta t = N/\Delta f$.

Equation [14] does not directly depend on either the bandwidth or the number of points acquired, only on the acquisition time. This dependence is plotted in Fig. 3. It can be seen that for an unfiltered FID the SNR has a maximum for an acquisition time of $T_{\text{AQ}} = 1.26 \cdot T_2^*$ (15).

To optimize the overall sensitivity of a sequence, the two above conditions must be combined by demanding that T_R be as short as possible, which means that $T_R \approx T_{\text{AQ}}$. Since then almost all the experiment duration is used for acquiring data, the time is used most effectively. Eq. [12] then becomes

$$\Psi = \frac{A(T_R) \cdot T_2^* \cdot (1 - e^{-T_R/T_2^*})}{a \cdot T_R}. \quad [15]$$

Again, we assumed the Ernst angle to be used. This relation is plotted in Fig. 4. The total maximum of the sensitivity is achieved for a repetition and acquisition time of between $1.2T_2^*$ and $1.3T_2^*$, the exact value depending on T_R , T_1 , and T_2^* . A further reduction of the acquisition and repetition time will result in a lower sensitivity.

Spin Echoes

Up to here only FID sequences were considered. The results, however, can easily be transferred to spin echoes by deriving expressions that describe the echo amplitude A_{echo} and the echo area f_{echo} , which replace the corresponding terms for FIDs. Then, Eq. [12] can be used for examining the sensitivity.

To calculate the amplitude A of the spin echo, we consider a sequence which consists of a $(180^\circ - \alpha)$ excitation pulse and a 180° refocusing pulse after a time $T_E/2$. At the time

T_E , the echo reaches its maximum amplitude, which can be calculated in a manner similar to the calculation of A_{FID} , yielding the result

$$\begin{aligned}
 A_{\text{echo}}(T_R, T_E, \alpha) &= M_0 \cdot e^{-T_E/T_2} \\
 &\times \frac{1 - e^{-T_R/T_1} + 2e^{-(T_R-1/2T_E)/T_1} - 2e^{-(T_R-3/2T_E)/T_1}}{1 - \cos \alpha \cdot e^{-T_R/T_1}} \\
 &\times \sin \alpha. \tag{16}
 \end{aligned}$$

The difference between Eqs. [3] and [16] is due to the delay between the excitation and the refocusing pulse: Since the refocusing pulse inverts the longitudinal magnetization, the T_1 relaxation during this time does not enhance but reduces the amplitude of the next signal. For short echo times, however, this period is very short and A_{echo} approaches A_{FID} . The difference between these two functions is therefore important only if long echo times are used, as is often the case in CSI. The angle α which yields maximal signal is the same as the Ernst angle for FIDs.

To derive the expression f_{echo} , we assume fully sampled, symmetrical spin echoes with $T_2 \gg T_2^*$. The FID signal in Eq. [6] then must be replaced by an echo: Instead of a pure decay it consists of a rise in the first half ($t < 0$) and a decay for $t > 0$; the exponential is $e^{-|t|/T_2^*}$. The integration of Eq. [6] then must be performed symmetrically from $-T_{\text{AQ}}/2$ to $T_{\text{AQ}}/2$. The result is

$$f_{\text{echo}}(T_{\text{AQ}}, \Delta f) = 2T_2^* \cdot \Delta f \cdot (1 - e^{-T_{\text{AQ}}/2T_2^*}). \tag{17}$$

The optimum acquisition time for an unfiltered spin echo is just twice that of an FID, $T_{\text{AQ}} = 2.52T_2^*$ (16; Fig. 3).

The result of the optimization of the repetition time for spin echoes is quite different than for FIDs: Putting Eq. [16] into [13] yields the magnetization accumulated in a given

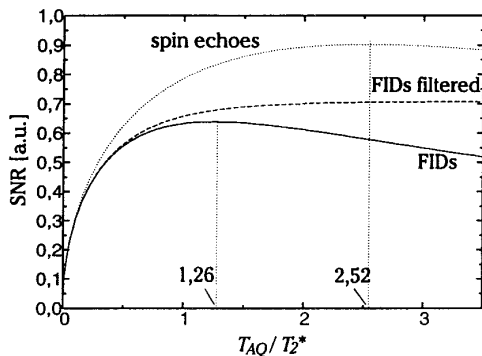


FIG. 3. Dependence of the SNR, Eq. [14], on the acquisition time for FIDs (straight line), FIDs with matched filter (broken line), and unfiltered echoes (dotted line). The maxima for unfiltered FIDs and echoes are marked.

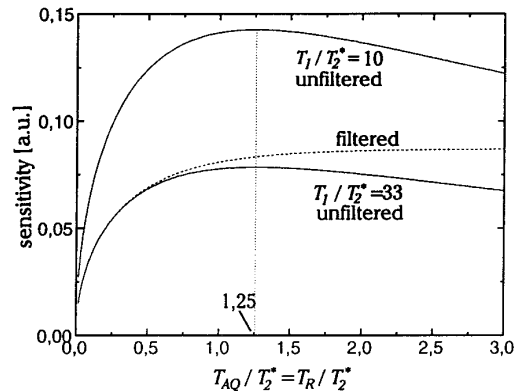


FIG. 4. Sensitivity of an FID experiment for two different T_1/T_2^* ratios as a function of the acquisition time. For $T_1/T_2^* = 33$ also the sensitivity using a matched filter is shown.

time, depending on T_R (Fig. 2). It reaches a maximum for repetition times between T_1 and $2T_1$. The exact value depends on both T_1 and T_E . For optimal sensitivity, the spin system requires more time for relaxation because the T_1 effect during the first half echo time reduces the longitudinal magnetization after the refocusing pulse. Since T_1 is usually much greater than T_2^* , the optimal repetition time is much longer than the optimal acquisition time of an unfiltered echo. These two parameters can therefore be optimized independently.

For short T_2 , the echoes often cannot be sampled symmetrically because an echo time of $T_{\text{AQ}}/2$ would be too long. Then spin echoes with very short echo times can be used, only the decaying parts of which are acquired. The shape of such a half spin-echo signal is similar to that of an FID and therefore is described by f_{FID} , and its amplitude is described by A_{echo} . Since very short echo times are used, A_{echo} is in these circumstances very similar to $A_{\text{FID}} \cdot e^{-T_E/T_2}$, the sensitivity of this experiment therefore is—except for the factor e^{-T_E/T_2} —totally described by the corresponding formulas for FIDs. The results derived there for optimum acquisition and repetition times are valid.

Multi-echo Experiments

A frequently used method for enhancing the SNR in a spin-echo experiment is to generate several echoes after each excitation by applying several refocusing pulses with spacing T_E . This way, the waiting period between acquisition and the start of the next repetition, which according to the previous section is necessary for optimal sensitivity, can be used to increase the signal intensity. We now want to find out how many echoes should be used for optimizing the SNR (17).

In the course of the echo train, the amplitude of the echoes goes down as e^{-mT_E/T_2} , m being the number of the echo. Acquisition of M echoes thus enhances the total signal by a

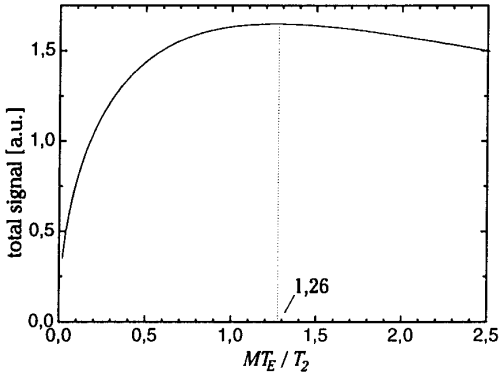


FIG. 5. Course of the accumulated signal for multiecho experiments as a function of the number of echoes M and the echo time T_E .

factor of $\sum_{m=1}^M e^{-mT_E/T_2}$, while the noise grows by \sqrt{M} . The total SNR improvement is found by dividing these expressions; the result is plotted in Fig. 5. There is a maximum for a total time between the first and the M th echo of $T_{\text{Etot}} = MT_E = 1.26T_2$. For an acquisition time of T_{AQ} this amounts to an optimal number of echoes of

$$M_{\text{opt}} = \frac{T_{\text{Etot}}}{T_{\text{AQ}}} = \frac{1.26 \cdot T_2}{T_{\text{AQ}}}. \quad [18]$$

Time Domain Filtering in the Spectral Dimension

In a spectroscopic experiment, the acquisition time is usually much longer than T_2^* in order to achieve the desired spectral resolution. To avoid loss in sensitivity due to this long acquisition, an exponential filter $e^{-t/b}$ is applied to the FID prior to Fourier transformation. It reduces the contribution of the noisy later part of the FID in favor of the beginning, where the signal is strong. For optimum sensitivity enhancement, the parameter b should be equal to T_2^* (“matched filter” (18)). The influence of this filter can easily be included in the formulas derived above by replacing f_{FID} by

$$f_{\text{filter}}(T_{\text{AQ}}, \Delta f) = \Delta f \cdot \sqrt{\frac{T_2^* \cdot T_{\text{AQ}}}{2}} (1 - e^{-2T_{\text{AQ}}/T_2^*}). \quad [19]$$

In Fig. 3 it can be seen how filtering removes the decay in sensitivity which otherwise takes place for acquisition times longer than $1.26T_2^*$. For $T_{\text{AQ}} = 2T_2^*$ this results in an SNR gain of 15%, for $T_{\text{AQ}} = 3T_2^*$ of 29%. If this kind of filtering is used, acquisition times longer than $1.26T_2^*$ hardly affect the sensitivity. Shorter acquisition times, however, should still be avoided.

While for half spin echoes filtering produces the same effect as for FIDs, whole spin echoes must be considered separately: here, we must filter with $e^{t/b}$ in the first and with

$e^{-t/b}$ in the second half of the echo. Again the best result is achieved with $b = T_2^*$, giving

$$f_{\text{echo, filter}}(T_{\text{AQ}}, \Delta f) = \Delta f \cdot \sqrt{T_{\text{AQ}} \cdot T_2^*} \cdot (1 - e^{-T_{\text{AQ}}/T_2^*}). \quad [20]$$

As in the case of FIDs, filtering increases the sensitivity for acquisition times that are longer than the optimum for the unfiltered case.

Read Gradients and Gradient Echoes

We will now analyze the influence of pulsed magnetic field gradients used to encode the spatial information on the sensitivity. In CSI, two methods for encoding spatial information are commonly used: “Phase gradients” are turned on for a short time prior to acquisition to introduce a space-dependent phase to the FID or echo. “Read gradients” are applied during data acquisition, in order to change the frequency of the signal as a function of its spatial origin. Fast CSI methods make use of read gradients in order to reduce the total duration of the experiment. We will show in the following that for spatially encoded signals, sampled in the presence of a read gradient, the formulas derived above for the spectral dimension are still valid.

In the presence of a read gradient G , the necessary bandwidth grows with the gradient strength and the field of view X as $\Delta f = (\gamma/2\pi) \cdot G \cdot X$, reducing the acquisition time $T_{\text{AQ}} = N/\Delta f$. According to Eq. [4], the noise amplitude increases with growing bandwidth. To analyze the influence of a gradient on the sensitivity, we examine the signal of a point source at x_0 , acquired in the presence of a read gradient G :

$$s(t) = A \cdot e^{-t/T_2^*} \cdot e^{i\gamma G t x_0}. \quad [21]$$

The second exponential describes the change of frequency due to the gradient. Our definition of T_2^* does not include the effects of applied field gradients; it describes only the reduction of the signal due to T_2 relaxation and B_0 inhomogeneities. It can thus be much longer than the apparent signal decay, which for extended sources is much stronger in the presence of a read gradient. In the Fourier transformation with

$$S(x) = \frac{1}{\Delta t} \cdot \int s(t) e^{-i\gamma G t x} dt \quad [22]$$

(as in Eq. [6] the factor $1/\Delta t$ must be added to take the discrete nature of the data into account) for $x = x_0$ the two exponentials in Eqs. [21] and [22] cancel, and the signal becomes

$$S(x_0) = A \cdot \frac{1}{\Delta t} \cdot \int_0^{T_{\text{AQ}}} e^{-t/T_2^*} dt = A \cdot f_{\text{FID}}(T_{\text{AQ}}, \Delta f). \quad [23]$$

This integral is identical to that in Eq. [6]. Although the noise amplitude is higher because of the larger bandwidth (Eq. [9]), the SNR as before is given by Eq. [14], which is independent of the bandwidth. The read gradient thus has no influence on the SNR, which depends in exactly the same way on the acquisition time as in the spectroscopic dimension. The modulation of the signal in the time domain in the presence of gradients is the carrier of the spatial information and thus disappears in the Fourier transformation. The higher noise amplitude in the presence of read gradients is just balanced by the signal gain because of the larger number of sampled data points which are accumulated. The results derived for the spectral dimension can therefore also be applied on the spatial domain. Though this result may seem surprising, it is actually well known by the spectroscopist: The SNR of a spectral line does not depend on the bandwidth, as long as the acquisition time remains the same. Read gradients in imaging do not alter this effect.

Very often it is said that imaging gradients do deteriorate the SNR, and the more the stronger they are. Such a statement does not contradict the above findings as it may appear at first glance, but it relies on a different assumption: Usually, the number of voxels in an image is kept constant, and the acquisition time consequently is reduced with increasing read gradient strength. This leads to a decreased SNR, which actually can be calculated exactly by Eq. [14]. Basing the sensitivity argument on the acquisition time rather than on gradient strength or bandwidth, however, makes it easier to find the optimal parameters for a good SNR. As shown above, best sensitivity is reached for $T_{AQ} = 1.26T_2^*$ (or $T_{AQ} = 2.52T_2^*$ for spin echoes), which is much longer than generally used in imaging. This optimal acquisition time can be realized either by applying a rather weak read gradient or by oscillating a strong read gradient and acquiring an adequate number of gradient echoes (19).

Phase Gradients

Phase gradients, applied between excitation and acquisition, encode the spatial information in a manner that is mathematically similar to the acquisition of a signal in the presence of a read gradient, as described by Eq. [23]. Since every phase encode step, however, is done on a separate signal, the T_2^* weighting in Eq. [23] must be replaced by the weighting of the individual phase encode steps, depending, for instance, on T_1 or T_2 . Most frequently, only one phase encoding gradient is applied per excitation, and the signals for all phase encoding steps are weighted equally. This case is described by setting the T_2^* in Eq. [23] to infinity, resulting in a total signal of $S(x) = A \cdot M$, with M being the number of phase encode steps. Phase encoding thus has the same effect on the sensitivity as averaging, as long as the voxel size remains constant.

Up to now we have argued for a sample consisting only of point sources. In extended sources, phase dispersion occurs

within every voxel, which causes a signal loss of 13% for every encoded dimension for symmetrical k -space sampling (20). Since this loss is inherent to and constant in all Fourier methods, it does not have to be considered in a comparison of methods.

II. METHODS OF FAST CHEMICAL SHIFT IMAGING

In addition to the classical CSI method (7, 21), several sequences for fast CSI experiments have been proposed. Their main goal is to reduce the experiment duration, especially for high spatial resolutions. Most of these methods are based on fast imaging sequences, which are modified in order to include the spectroscopic information. We will now apply the results of the previous section to some of these methods.

Following the considerations of the preceding section, an equation for calculating the sensitivity of an experiment with two spatial dimensions is found as

$$\Psi = \frac{1}{N_x N_y} \cdot \frac{A \cdot f_x \cdot f_y \cdot f_\delta \cdot V_{\text{prep}}}{\sqrt{N_x N_y N_\delta \Delta f} \cdot \sqrt{T_{\text{tot}}}} \quad [24]$$

The first term describes the voxel size: For a constant sample volume, the size and thus the signal originating in one voxel goes down with an increasing number of voxels in the x and y direction. The amplitude of the FID or the echo in the time domain is represented by the factor A , which in most cases is given by Eqs. [3] or [16]. For some methods, however, A needs to be extended to describe the maximum amplitude of the time domain signal. The terms f_x , f_y , and f_δ describe the effect of the Fourier transformation on the signal in the two spatial and one spectral dimension and are usually given by one of the Eqs. [7] or [17], but also different values are possible. V_{prep} is an additional, method-dependent factor which describes processes during the preparation period of the experiment. The square roots in the denominator are the noise amplitude, Eq. [9], and the total time needed for the experiment, $T_{\text{tot}} = N_{\text{rep}} \cdot T_R$, N_{rep} being the total number of repetitions.

To avoid excessive calculations, only for the first method are all terms in Eq. [24] derived in detail. The sensitivity of the other experiments is then estimated by comparison to methods treated before. A quality factor Ω which relates the sensitivity of all fast methods to the classical CSI sequence as a function of the relevant experimental parameters is defined:

$$\Omega_{\text{sequence}} = \frac{\Psi_{\text{sequence}}}{\Psi_{\text{CSI}}} \quad [25]$$

Emphasizing the differences between the methods, this quality factor allows one to concentrate on the parameters which have changed from one method to the other. For a

TABLE 1
The Parameters of the Model Experiment

Static magnetic field	B_0	1.5 T
Gyromagnetic ratio (protons)	γ	$267.54 \times 10^6 \text{ s}^{-1} \text{ T}^{-1}$
Resonance frequency	ν_0	63.9 MHz
Longitudinal relaxation time	T_1	1 s
Transversal relaxation time	T_2	300 ms
Apparent relaxation time	T_2^*	30 ms
Spectral range	$\Delta\delta$	639 Hz = 10 ppm
Spectral resolution	N_δ	64
Spectral dwell time ^a	Δt_δ	1.6 ms
Spectral acquisition time ^b	$T_{AQ\delta}$	100 ms
Field of view in the x and y direction	X, Y	25 cm
Spatial resolution in the x and y direction	N_x, N_y	32
Phase encoding time	τ_G	2 ms
Gradient rise time	τ_w	500 μs
Soft pulse duration	τ_p	5 ms
For a read gradient strength of 1 mT/m ^c		
Bandwidth ^d	Δf	11284 Hz
Spatial dwell time ^e	Δt_x	88.6 μs
Gradient echo duration ^f	T_{AQx}	2.8 ms

^a Spectral dwell time: $\Delta t_\delta = 1/\Delta\delta$.

^b Spectral acquisition time: $T_{AQ\delta} = N_\delta \cdot \Delta t_\delta$.

^c The parameters bandwidth, spatial dwell time, and gradient echo duration depend on the gradient strength, which is optimized for each method. Only if this optimization results in a gradient strength G of less than 1 mT/m are the listed values used.

^d Bandwidth: $\Delta f = N_x \cdot G + \Delta\delta$.

^e Spatial dwell time: $\Delta t_x = 1/\Delta f$.

^f Gradient echo duration: $T_{AQx} = N_x \cdot \Delta t_x$.

complete quantitative analysis, the values of the different factors in Eq. [24] for each method analyzed are listed in Table 2.

The Model Experiment

In addition to computing the abstract sensitivity formulas for all fast CSI methods shown in Fig. 6, we also applied them to a model CSI experiment on a 1.5-T whole-body instrument. The parameters assumed in this experiment are listed in Table 1. They correspond to a typical ¹H CSI measurement in the human brain. A linewidth of 10 Hz has been assumed, corresponding to an apparent relaxation time T_2^* of 30 ms. For each method, the optimal excitation angle, echo time, acquisition time, and repetition time under the given experimental conditions were selected. The relative sensitivity as a function of the spectral resolution is drawn for all sequences in Fig. 7a, and the minimal experiment duration as a function of the spatial resolution is shown in Fig. 7b.

Calculating the optimal acquisition time for sequences, where only one gradient echo is acquired per repetition, one finds a rather low strength of the read gradient: Using Eq. [7] we get for the apparent relaxation time T_2^* of 30 ms

assumed in the experiment an optimum acquisition time of 38 ms. For a spatial resolution of 32 points this implies a read gradient strength of only 19 $\mu\text{T/m}$. NMR imaging, however, requires stronger gradients to avoid image distortions which are caused by B_0 inhomogeneities or by susceptibility differences. We therefore assume a minimum read gradient strength of 1 mT/m.

The Classical CSI Experiment

The first and most commonly used method is the classical CSI experiment (7, 21; see Fig. 6a). The spatial information is encoded solely by phase encoding in all spatial dimensions, and the signal is acquired in the absence of magnetic field gradients. If the experiment is performed as a single-pulse excitation sequence, observing FIDs, the sensitivity is determined by the following factors:

The amplitude of the FID right after the excitation pulse is given by $A_{\text{FID}}(\alpha, T_R)$, Eq. [3]. The initial amplitude of the acquired signal, however, is reduced by a factor of $V_{\text{prep}} = e^{-\tau_G/T_2^*}$ due to the T_2^* decay during the time τ_G needed for phase encoding.

As shown above, the effect of N_x phase encoding steps is a signal enhancement by N_x , giving rise to the factors $f_x = N_x$ and $f_y = N_y$. The Fourier transformation in the spectral dimension causes a factor $f_\delta = f_{\text{FID}}(T_{AQ}, \Delta\delta)$. Since no read gradients are used, the bandwidth Δf in Eq. [7] is equal to the frequency range $\Delta\delta$ of the spectrum.

The total duration of the experiment is

$$T_{\text{tot}} = N_x N_y T_R. \quad [26]$$

Putting all parameters into Eq. [24], we get the result

$$\Psi_{\text{CSI}} = \frac{A_{\text{FID}}(\alpha, T_R) \cdot e^{-\tau_G/T_2^*}}{aN_x N_y \sqrt{N_\delta} \cdot \Delta\delta \cdot T_R} \cdot f_{\text{FID}}(T_{AQ}, \Delta\delta). \quad [27]$$

The highest sensitivity is achieved by minimizing the repetition time and using the Ernst angle for excitation. This variant is called FLASH-CSI (22) and optimizes the sensitivity at the cost of a strong T_1 weighting. The repetition time then is $T_R = T_{AQ} + \tau_G$.

The sensitivity of this experiment as a function of the spectral resolution for our model experiment is plotted in Fig. 7a. Since the spectral resolution is proportional to the acquisition time, this graph has the same shape as that in Fig. 3, having a maximum for an acquisition time of 1.26 T_2^* . The sensitivity decay for long repetition times, however, is only small and can be removed by filtering. Figure 7b shows the time needed for the experiment which can be quite long for a high spatial resolution because of the high number of phase encode steps required.

The time τ_G , which is needed to perform the phase encoding, also introduces a phase factor which cannot easily be removed without distortion of the spectrum (23). This prob-

TABLE 2
Result of the Calculation and Optimization of the CSI Methods, Using the Formalism of Eq. [24]

Method	A	V_{prep}	f_x	f_y	f_δ	T_w^a	Δf_{opt}^b	N_{rep}^a
Classical CSI	A_{FID}^c	$e^{-\tau_g T_2}$	N_x	N_y	f_{FID}^e	0	$\Delta\delta$	$N_x N_y$
SE-CSI	A_{echo}^d	—	N_x	N_y	f_{echo}^f	$> T_1$	$\Delta\delta$	$N_x N_y$
Echo-time encoding	A_{echo}	—	f_{FID}	N_y	f_{echo}	$> T_1$	Small ^b	$N_\delta N_y$
SPLASH	A_{FID}	$e^{-2\tau_g T_2}$	f_{FID}	N_y	f_{FID}	0	Small	$N_\delta N_y$
SNAP	A_{snap}^h	1/2	f_{FID}	M_{rel}^h	f_{FID}	$> T_1$	Small	N_δ
PREP	A_{FID}	—	f_{FID}	N_y	f_{FID}	0	$\frac{N_x \Delta\delta}{1 - \Delta\delta \tau_s}$	N_y
PEEP	A_{echo}	—	f_{FID}	N_y	f_{echo}	$> T_1$	$\frac{N_x \Delta\delta}{1 - \Delta\delta \tau_s}$	N_y
U-FLARE	$(1 - e^{-T_w/T_1}) \sin \frac{\beta}{2}$	e^{-T_d/T_1}	f_{FID}	$e^{-\sum_{n=1}^{N_y} n T_r/T_1}$	f_{FID}	$> T_1$	Small	N_δ
EBI	$\frac{A_{\text{echo}}}{\sqrt{N_\delta}}$	—	f_{FID}	N_y	f_{echo}	$> T_1$	$2N_x \Delta\delta$	N_y
EPSM	1	—	f_{FID}	f_{FID}	f_{FID}	—	$\frac{\Delta\delta N_x N_y}{1 - \Delta\delta N_y \tau_s}$	1
SISSI	$e^{-T_E/T_2/\sqrt{N_\delta}}$	—	f_{FID}	N_y	f_{echo}	—	$\frac{N_x N_y}{\Delta t_\delta - \tau_s}$	1

Note. For further explanation of symbols see the text and Fig. 6.

^a T_w is the optimum relaxation time between two repetitions of the experiment, and N_{rep} the total number of repetitions. The total experiment duration T_{tot} is calculated by adding T_w to the duration of one repetition and multiplying by the number of repetitions N_{rep} .

^b Δf_{opt} is the optimum bandwidth. For experiments where a single gradient echo is acquired, the sensitivity optimization yields a gradient far lower than corresponds to a gradient of 1 mT/m, which is not practicable in NMR. Then ‘‘small’’ means that the bandwidth corresponding to the weakest possible gradient is best.

^c A_{FID} is defined by Eq. [3].

^d A_{echo} is defined by Eq. [16], where the echo time $T_E = T_{\text{AQ}\delta}$, except for EBI, where $T_E = T_{\text{AQ}\delta}/2$.

^e f_{FID} is defined by Eq. [7].

^f f_{echo} is defined by Eq. [17].

^g T_d is the time needed for dummy scans (necessary for U-FLARE with small refocusing angles).

^h $A_{\text{snap}} = M_{\text{rel}} \cdot (1 - e^{-T_r/T_1}) \cdot e^{-T_w/T_1} + 1 - e^{-T_w/T_1}$ and $M_{\text{rel}} = \sum_{n=0}^{N_y-1} e^{-nT_r/T_1} \cos^n \alpha$, where T_r is the repetition time during the imaging part of the sequence.

lem is avoided when a spin-echo sequence is used. The phase gradients can then be applied before the refocusing pulse (see Fig. 6b). The sensitivity of spin-echo CSI can easily be derived from Eq. [27], by replacing the FID terms by those for spin echoes:

$$\Psi_{\text{SE-CSI}} = \frac{A_{\text{echo}}(\alpha, T_R, T_E)}{a N_x N_y \sqrt{N_\delta} \cdot \Delta\delta \cdot T_R} \cdot f_{\text{echo}}(T_{\text{AQ}}, \Delta\delta). \quad [28]$$

The quality factor $\Omega_{\text{SE-CSI}}$ is now found by dividing this equation by Eq. [27], where the different optimal repetition times must be observed. Since the T_R optimization yields a much higher repetition time for echoes than for FIDs (Fig. 2), the total experiment duration is longer.

Whether the spin echo or the FID experiment has a higher sensitivity depends on the value of T_2 : The factor f is higher for echoes than for FIDs, because a larger part of the acquired signal has a high amplitude. The A factor, however, is smaller for echoes by an amount that depends on the T_2 relaxation. For the T_2 value of 300 ms chosen for the model experiment, the sensitivity of the FID experiment is usually lower than for echoes (Fig. 7a). Since we assume symmetrically sampled echoes, a high spectral resolution yields a long

echo time. Then, the T_2 loss is quite large and the sensitivity falls below that of the FID variant.

For long T_2 values the extension to a multiecho sequence can be advantageous (24). The long repetition time necessary for spin-echo experiments then is used to enhance the SNR or to reduce the duration. However, the results derived above for multiechoes should be observed: According to Eq. [18], a number of four echoes per excitation yields the highest sensitivity for the model experiment.

Echo-Time Encoding

The main drawback of the classical CSI experiment is the large number of repetitions needed for high spatial resolutions. The minimal duration of such an experiment is unacceptable for many applications. The following method was developed in order to increase the speed of the experiment for high spatial but low spectral resolutions (25, 26). It requires $N_\delta \cdot N_y$ repetitions instead of the $N_x \cdot N_y$ needed in classical CSI. This sequence (see Fig. 6c) utilizes a read gradient for spatial encoding in one direction. The position of this gradient is in subsequent repetitions shifted by a variable time t_δ with respect to the maximum of the spin echo, thus

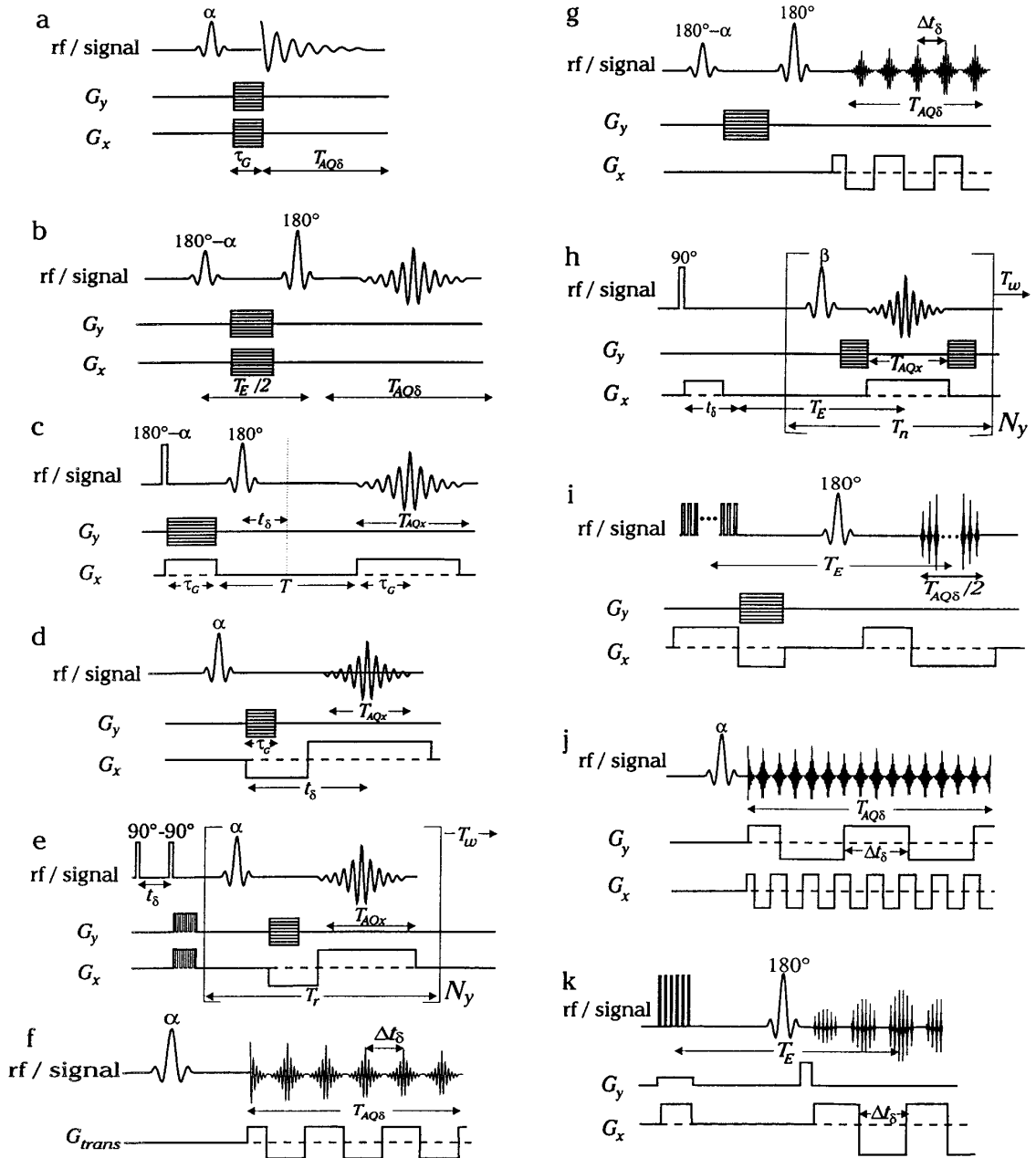


FIG. 6. Pulse sequences of the treated methods: (a) classical CSI, (b) SE-CSI, (c) echo-time encoding, (d) SPLASH, (e) spectroscopic SNAP, (f) PREP, (g) PEEP, (h) spectroscopic U-FLARE, (i) EBI, (j) EPSM, (k) SISSI. In all sequences, the slice gradient is omitted for simplicity.

encoding the spectral information. A phase gradient is used for resolving the second spatial dimension.

The sensitivity of this experiment can be found by comparison to the spin-echo variant of classical CSI: Instead of phase encoding, one of the spatial dimensions is resolved by applying a read gradient. The factor N_x in Eq. [27] thus is replaced by the signal of a gradient echo, $f_x = f_{\text{FID}}(T_{\text{AQ}}, \Delta f)$. Since the acquisition time in the presence of a read gradient usually is much shorter than T_2^* even for quite small gradients, this factor is approximately equal to N_x , which is the same as for phase encoding. The signal amplitude of

both methods thus is the same. The larger bandwidth Δf required in the presence of read gradients, however, increases the noise compared to that of classical CSI by a factor $\sqrt{\Delta f / \Delta \delta}$. Since in both cases spin echoes are used, the repetition time is equal, and the total experiment time thus differs by a factor N_δ / N_x , and the total sensitivity by

$$\Omega_{\text{echo time}} = \sqrt{\frac{\Delta \delta \cdot N_x}{\Delta f \cdot N_\delta}} \cdot \Omega_{\text{SE-CSI}}. \quad [29]$$

For small spectral and high spatial resolutions, N_x / N_δ be-

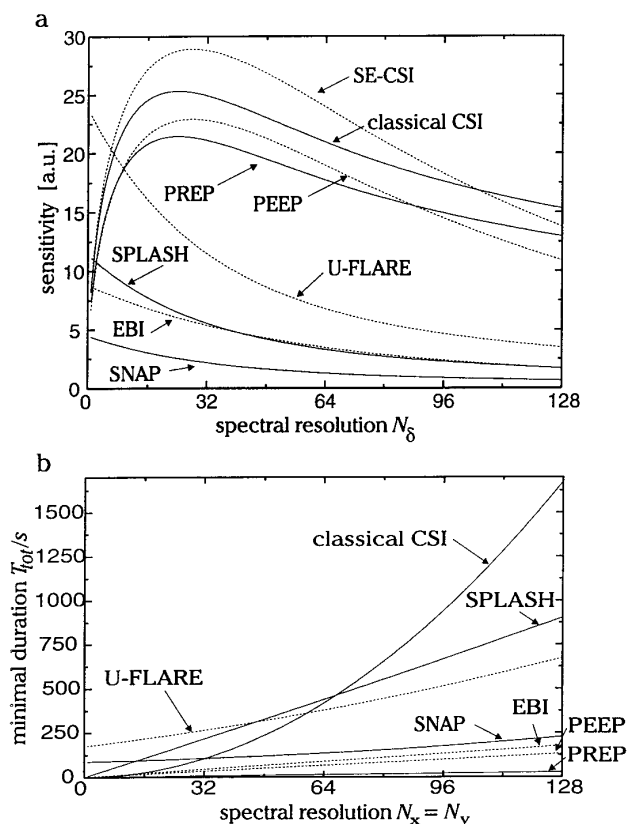


FIG. 7. Sensitivity and minimal experiment duration for the CSI methods compared. (a) Sensitivity as a function of the spectral resolution. (b) Experiment duration as a function of the spatial resolution. All other parameters are fixed according to Table 1. The broken lines indicate spin-echo methods.

comes larger than $\Delta\delta/\Delta f$ and the sensitivity of this method exceeds that of the classical CSI experiment. This can be realized by using specially adjusted phase gradients to make separate images of only two chemical shift species (e.g., water and fat; 27). This method is, furthermore, the base of faster experiments to be presented in the following sections.

The model experiment used for Fig. 7 has a quite high spectral resolution; the sensitivity of this sequence thus is much weaker than that of other methods.

FLASH-Based Techniques

The fast methods we will present in the following sections are derived from fast imaging methods, which are modified to introduce the chemical shift information. Three CSI modifications of the FLASH (fast low angle shot) imaging sequence (28, 29) are treated here. These are FLASH-CSI, which has already been presented as an optimized version of classical CSI, as well as SPLASH and spectroscopic snapshot-FLASH.

SPLASH

The SPLASH (spectroscopic FLASH) sequence (30; Fig. 6d) consists of a gradient echo, the position of which is

shifted with reference to the excitation pulse by a variable delay t_δ in N_δ subsequent repetitions. Similar to echo-time encoding, one spectral point is sampled per repetition, already resolved in one spatial dimension. The second spatial dimension is phase encoded by a gradient between excitation and acquisition. For an entire experiment, $N_\delta \cdot N_y$ repetitions are needed, and in each of them a gradient echo with N_x points is acquired. The repetition time is equal to that of FLASH-CSI, resulting in a difference in the total duration of $T_{\text{CSI}}/T_{\text{SPLASH}} = N_\delta/N_x$. The sensitivity, however, is reduced due to the read gradient, which requires a far larger bandwidth and thus increases the noise amplitude by a factor $\sqrt{\Delta f/\Delta\delta}$. The total difference in sensitivity of these two experiments thus is

$$\Omega_{\text{SPLASH}} = \sqrt{\frac{\Delta\delta \cdot N_x}{\Delta f \cdot N_\delta}}. \quad [30]$$

Since Δf is much higher than $\Delta\delta$, SPLASH can achieve a higher sensitivity than CSI only for a very small spectral and high spatial resolution.

Both sensitivity and duration of this experiment are plotted in Fig. 7 for the model experiment. The read gradient strength is assumed to be 1 mT/m.

Spectroscopic SNAP

The pulse sequence of the spectroscopic modification of snapshot-FLASH (SNAP; 31) is shown in Fig. 6e: In order to encode the chemical shift information, two 90° pulses, separated by a variable preparation period t_δ , are applied, and the remaining transversal magnetization is then destroyed by crusher gradients. The chemical shift information is now stored as amplitude modulation of the longitudinal magnetization. The spatial distribution of this component is finally measured using a fast snapshot-FLASH imaging sequence. With each repetition a whole image is acquired; only N_δ repetitions with varying preparation times t_δ are necessary.

Here, the spectroscopic information is stored in the amplitude of the longitudinal magnetization as deviation from the steady state. The assumption made for the other experiments, that the spin system is in the steady state, described by Eq. [3], cannot be applied. To calculate the signal amplitude of this experiment, we thus must observe the course of the signal toward equilibrium during the FLASH sequence and determine again the optimum values for repetition time and flip angle. The results of exact calculations are shown in Fig. 7. Here, instead of going through all the steps of the quite complicated calculations, we restrict ourselves to some qualitative statements to explain the strongly reduced performance in comparison to other methods.

In a normal FLASH imaging sequence, the longitudinal magnetization that is generated due to T_1 relaxation during the experiment contributes to the signal. In the spectroscopic version this magnetization is lost, since it does not contain

the spectroscopic information. It is not modulated by the preparation pulses and therefore does not contribute to the spectrum, but gives rise to a line with frequency zero. The amplitude of the desired spectroscopic signal decreases in the course of the imaging sequence, which for the parameters of the model experiment amounts to a total loss in signal of about 1/2.

An additional signal reduction of another 1/2 is due to the fact that the chemical shift information is stored only in the amplitude, and not also in the phase of the signal.

In spite of the very low duration of this experiment, these effects reduce its sensitivity to about one-quarter of that of the SPLASH sequence. The quality factor of spectroscopic SNAP thus is

$$\Omega_{\text{SNAP}} \approx \frac{\Omega_{\text{SPLASH}}}{4}. \quad [31]$$

As explained above, the relevant part of the signal decreases in the course of the imaging experiment, thus introducing a certain weighting of the differently phase-encoded gradient echoes of each image. This causes a broadening of the pointspread function and thus affects the spatial resolution of the experiment.

EPI-Based Techniques

Echo planar imaging (EPI; 32) is the fastest imaging method, but is often affected by a short T_2^* because of its long acquisition time. In spectroscopic experiments, however, the spectral acquisition time is determined by the spectral resolution and is independent of the method that is used. All methods thus suffer equally from short T_2^* values. EPI variants are quite suitable for spectroscopic applications and several variations have been proposed, including PREP, PEEP and the single-shot method EPSM, which will be treated in a separate section.

PREP

The pulse sequence of PREP (projection-reconstruction echo planar imaging; 33, 34; see Fig. 6f) is similar to that of a normal EPI experiment with the phase gradient left out. An oscillating read gradient G_{trans} generates a train of N_δ gradient echoes with an echo spacing equal to the spectral dwell time Δt_δ , thus scanning a plane in k -space in the spectral and one spatial dimension at each repetition. The spatial resolution is performed by a projection-reconstruction scheme (35, 36): The direction of the oscillating gradient is rotated in subsequent repetitions, and the signal then is reconstructed with a back-projection algorithm, thereby avoiding the problems caused by a phase gradient put in between excitation and acquisition. The number of repetitions necessary for a resolution of N_x^2 points is approximately equal to N_x , with the same number of data points acquired in each gradient echo.

The sensitivity of this experiment is optimized by using short repetition times and the Ernst angle. The acquisition time is as long as in classical CSI. It could therefore in principle reach the same sensitivity. In realistic experiments, however, a finite time τ_s is needed for gradient switching. Since this time is not used for acquisition, the total acquisition time and thus the sensitivity is reduced. For an optimized gradient strength, where the gradients are such that one spectral dwell time is just used up with gradient switching and acquisition of the N_x points, this sensitivity loss amounts to

$$\Omega_{\text{PREP}} = \sqrt{1 - \tau_s \Delta \delta}. \quad [32]$$

In our model experiment, we assume gradient switching times of $\tau_s = 500 \mu\text{s}$ and a spectral width of $\Delta \delta = 639 \text{ Hz}$. For a field of view of 25 cm and a spatial resolution of 32 points a gradient strength of 2.8 mT/m is required. The factor $\sqrt{1 - \tau_s \Delta \delta}$ is then equal to 0.83, and the sensitivity of PREP thus is reduced by 17% with respect to that of classical CSI. It is, however, much faster, since only N_x repetitions are necessary (Fig. 7b).

The signal loss compared to classical CSI is caused only by the interruptions in the acquisition due to gradient switching and might be avoided by using alternative read gradient forms which allow efficient and continuous acquisition even during the gradient switching period (37). This, however, requires more complicated reconstruction methods.

PEEP

PEEP (phase-encoded echo planar imaging; 38; Fig. 6g) is the Fourier variant of PREP. Again one spatial and the spectroscopic dimensions are scanned simultaneously by an oscillating read gradient. The second spatial direction now is encoded by a phase gradient. The entire experiment is done as a spin-echo sequence, where the phase encoding is applied during the first half echo time. As for the spin-echo variant of classical CSI, this implies an optimal repetition time of about T_1 , and is therefore slower than the FID method PREP, although the same number of repetitions is necessary. The loss in sensitivity, now compared to classical spin-echo CSI, has the same amount and the same reasons as stated for PREP:

$$\Omega_{\text{PEEP}} = \sqrt{1 - \tau_s \Delta \delta} \cdot \Omega_{\text{SE-CSI}}. \quad [33]$$

The square root has for the model experiment again the value 0.83, indicating a 17% loss in sensitivity (Fig. 7).

A variation of this experiment is EPSI (echo planar spectroscopic imaging; 39), where water suppression and volume selection are added to perform *in vivo* measurements on the human brain.

Spectroscopic U-FLARE

The U-FLARE (ultrafast low-angle RARE) imaging sequence (40) is derived from the RARE (rapid acquisition

with relaxation enhancement) experiment (41), which uses a train of separately phase-encoded spin echoes sampled in the presence of a read gradient to generate strongly T_2 -weighted images. A 90° excitation pulse is applied, followed by N_y refocusing pulses. To reduce the applied RF power, the flip angles β of the refocusing pulses can be much smaller than 180° , which also reduces the T_2 weighting. The amplitude of an echo at the time t after excitation is $\sin(\beta/2) \cdot e^{-t/T'}$ (42). The time constant T' of the decay is equal to T_2 for $\beta = 180^\circ$, but longer for smaller refocusing angles, since a part of the magnetization is stored in the longitudinal direction (43).

The experiment can be modified for CSI applications by shifting the 90° excitation pulse in steps of Δt_δ in N_δ subsequent repetitions with respect to the first refocusing pulse (44; Fig. 6h). The spectroscopic information is then stored as phase modulation of the transverse magnetization and refocused in each of the spin echoes of the echo train. In each repetition a whole image consisting of N_y echoes is sampled for one point in the spectroscopic dimension. To separate the spin echo and the stimulated echo in the signal, a second, phase-cycled run of the entire experiment is necessary, which reduces the sensitivity by $1/\sqrt{2}$ (45). Since the longitudinal magnetization is to a great extent destroyed at the end of the spin-echo train, a relaxation period T_w of more than T_1 is necessary between two repetitions. In total, this method reaches a sensitivity of

$$\Omega_{\text{U-FLARE}} = \frac{(1 - e^{-T_w/T_1}) \cdot \sin(\beta/2) \cdot \sum_{n=1}^{N_\delta} e^{-nT_n/T'}}{A_{\text{FID}}(T_{\text{R-CSI}}, \alpha)} \times \sqrt{\frac{T_{\text{R-CSI}} \cdot \Delta\delta}{2N_\delta \cdot T_{\text{R}} \cdot \Delta f}}, \quad [34]$$

where $T_{\text{R-CSI}}$ is the repetition time used in the classical CSI experiment, to which this method is compared. The repetition time of the U-FLARE experiment is T_{R} , which consists of the preparation time, the time needed for the N_y echoes, and the relaxation period T_w . The first factor in the numerator replaces the $A(T_{\text{R}}, \alpha)$ term of other methods. It describes the relaxation of the longitudinal magnetization during T_w . The third term sums over the amplitudes of the echo train. T_n is the echo spacing.

For the model experiment (Fig. 7), a refocusing angle of $\beta = 180^\circ$ was chosen. Since U-FLARE is T_2 -weighted, its sensitivity can suffer strongly from a short T_2 . The decay during the echo train also causes a broadening of the point-spread function and thus affects the spatial resolution.

EBI

EBI (echo-time-encoded BURST imaging; 46) is a derivative of the BURST imaging sequence (47), where a fast train of low-angle excitation pulses is applied in the presence of a gradient in the read direction to generate the required

number of echoes. In EBI (Fig. 6i), a BURST excitation consisting of N_δ pulses is followed by a refocusing pulse and the signals are acquired as gradient echoes. Additional gradients in the read direction are applied to shift the position of the gradient echoes with respect to their respective spin-echo maxima: In the first gradient echo, the magnetization excited in the first pulse of the excitation is refocused, while its corresponding spin-echo maximum would be at the position of the last gradient echo. Only for the central echo is the spin-echo condition fulfilled. The gradient echoes are thus modulated by the overlying spin echo. Due to this scheme, the echo spacing is only $\Delta t_\delta/2$ and the total acquisition time is only half that used in a classical CSI experiment. This reduces the sensitivity by a factor of $1/\sqrt{2}$ because stronger gradients are required.

A further reduction of the sensitivity is due to the BURST excitation scheme, which does not excite the sample uniformly. By optimally phasing the BURST pulses (“chirp” pulse; 48), an echo amplitude that is $1/\sqrt{N_\delta}$ of the signal of a simple 90° excitation pulse (49) can be reached. These arguments add up to a quality factor of

$$\Omega_{\text{EBI}} = \frac{\Omega_{\text{SE-CSI}}}{\sqrt{2N_\delta}}. \quad [35]$$

This result is plotted for the model experiment in Fig. 7.

Single-Shot Methods

Because of the small concentrations of the metabolites observed in CSI, most experiments require several averages to accumulate the SNR needed. In some cases, however, when the signal is high, the spatial resolution is low, and the experiment must be very fast, even the use of single-shot methods can be useful, where only one excitation is necessary to acquire all the necessary data. They have the advantage of high speed, combined with a high sensitivity, which arises because if only one excitation is needed, all the equilibrium longitudinal magnetization is available. This advantage, however, is lost as soon as several repetitions are needed for averaging. The sensitivities calculated in the following sections thus are valid only if they really are used as single-shot experiments. Otherwise, each of the multishot sequences treated earlier reaches a higher sensitivity and is easier to implement.

Two single-shot sequences will be treated: the EPI variant EPSM and the BURST derivative SSSI.

EPSM

The pulse sequence of EPSM (echo-planar shift mapping; 34, 50; see Fig. 6j) is derived from PREP by adding a second gradient, which is inverted after N_y oscillations of the first one. The gradients must be fast enough to acquire a whole image in only one spectral dwell time Δt_δ . This

way, a series of N_δ images with spacing Δt_δ is made from only one FID. This method thus requires extremely strong and fast gradients and nevertheless allows only a very small spatial resolution. The sensitivity, however, can be quite high since the total longitudinal magnetization is excited by just one pulse with an angle of 90° . The frequent gradient switching points, however, use up the greatest part of the total acquisition time. The sensitivity depends on the square root of the acquisition time and thus decreases with increasing gradient switching time τ_s and number of switching points, which is determined by the spatial resolution. The quality factor thus is

$$\Omega_{\text{EPSM}} = \frac{\sqrt{1 - N_y \tau_s \Delta \delta}}{A_{\text{FID}}(T_{\text{R-CSI}}, \alpha)}. \quad [36]$$

The denominator describes the signal gain of the single-shot method compared to steady-state experiments with repetition time $T_{\text{R-CSI}}$, where only a part of the magnetization is available for every excitation.

Because of the strong requirements on the gradient system, the model experiment must be modified in order to be able to be realized as an EPSM experiment. For a spatial resolution reduced to 8×8 points and a gradient switching time of $150 \mu\text{s}$, a gradient strength of 15 mT/m is necessary. Even with these parameters, 77% of the acquisition time is actually used for gradient switching, thus reducing the sensitivity by 48% (Fig. 8).

In spite of its great sensitivity, the use of this method is strongly limited by its high demands on the instrument and restrictions on the resolution.

SISSI

Another single-shot sequence, SISSI (single-shot spectroscopic imaging; 51; Fig. 6k), uses a BURST excitation to generate a number of closely spaced gradient echoes, which are perpetually refocused by an oscillating read gradient. Similar to the EPSM sequence, this method can be used as either an FID or a spin-echo method. Its signal amplitude is degraded because of the BURST excitation by a factor of $1/\sqrt{N_y}$. The total acquisition time, however, is increased because only one gradient switching point per spectral dwell time is required. The restrictions on the gradient system thus are much lower than those for EPSM. The quality factor is

$$\Omega_{\text{SISSI}} = \sqrt{\frac{1 - \tau_s \Delta \delta}{N_y (1 - N_y \tau_s \Delta \delta)}} \cdot \Omega_{\text{EPSM}}. \quad [37]$$

The sensitivity of EPSM (Fig. 8) will in most cases exceed that of SISSI if fast gradient systems are used. The advantages of SISSI, however, are the far lower requirements on the gradient system and the much easier implementation.

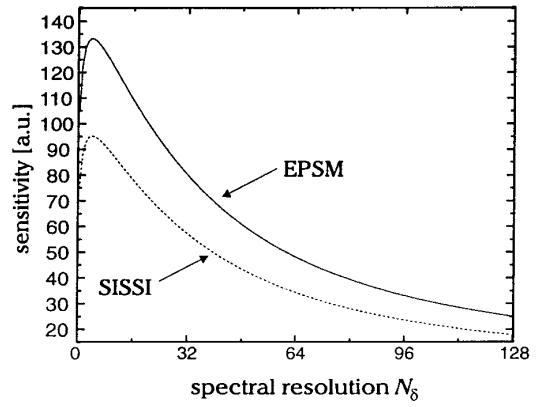


FIG. 8. Sensitivity of the single-shot methods EPSM and SISSI. A modified model experiment was assumed (see text).

DISCUSSION

The results plotted in Fig. 7 show the superiority with respect to the sensitivity of the classical CSI experiment. For a spatial resolution of 32×32 points and a repetition time of 1 s, this experiment takes about 17 min. Since such an experiment time is often needed anyway to reach the necessary SNR, the number of phase encode steps in that case does not impose a critical limitation on the experiment. Furthermore, if FIDs are observed the repetition time can be even further reduced. The sensitivity advantage of classical CSI can be explained by comparing its properties with the optimization criteria derived in the first section of this work: The long acquisition times per excitation as well as the possibility of easily optimizing the flip angle and the repetition time in FLASH-CSI yield the strongest possible signal. Furthermore, this method most effectively makes use of the signal that is present: Every FID or echo is entirely acquired from its beginning to its end, thus accumulating all the available signal. The acquisition duty cycle approaches 100%, which is ideal for optimal sensitivity.

The same arguments account for the almost as good performance of the EPI variants PREP and PEEP. The only loss of signal occurs because the acquisition must be stopped during the gradient switching times. This can be avoided by choosing gradient shapes that allow continuous sampling (37, 52). These schemes, however, employ an unfavorable k -space weighting which still affects the achievable signal gain.

Observing the results in Fig. 7, one should keep in mind that it only visualizes the results for a special model experiment. Different parameters can significantly change the relative performance of the various sequences. Most of all, the T_2 value and the spatial and spectral resolutions have a strong influence on the sensitivity. For all values, however, the sensitivity can be calculated using the equations given for the quality factor or in Table 2.

Furthermore, all results can easily be applied to three-

dimensional experiments: Although the minimal duration of an experiment grows significantly, the sensitivity remains the same as that for two dimensions, since a higher number of phase encode steps also enhances the signal intensity. To reduce the measuring time for such an experiment, for 3D applications as well as for correlation peak imaging (8, 9) fast sequences can be particularly useful. Fast methods can also be applied when dynamical processes are to be measured and a high signal is present. Then fast CSI allows a relatively good time resolution at the cost of a lower SNR (53).

Reducing the experimental duration by fast CSI methods not only affects the sensitivity, but also increases the technical difficulties. Fast gradient systems may be necessary and the processing of the data may be more difficult. Furthermore, artifacts can appear due to eddy currents. It should also be noted that in addition to the sensitivity, there are other factors which influence the quality of an experiment. One of them is the achievable spatial resolution: For classical CSI, where only phase encoding is used, the spatial resolution is insensitive to chemical shift and susceptibility, which can become a problem when acquiring under a gradient. Furthermore, in some fast methods the phase encode steps are differently weighted, which affects the spatial resolution by broadening the spatial response function. On the other hand, fast methods can prevent blurring which is caused by motion.

Naturally, this comparison of methods could not cover all published sequences: Different methods (54–56) or variations of those treated here have been reported.

CONCLUSION

The gold standard for sensitivity is set by the conventional CSI experiment. Depending on the T_2 relaxation time, pulse-acquire or spin-echo sequences are advantageous. Fast CSI sequences do not improve the sensitivity, which remains the main factor limiting the achievable spatial resolution. They allow one to shorten the minimal duration of the experiment only in situations where either the available signal is strong or a very high resolution is required (i.e., in three-dimensional CSI). They can also be advantageous in circumstances where the spatial localization of classical CSI is blurred by motion or similar effects.

We have presented criteria which allow one to evaluate fast CSI sequences for any given experimental conditions and to choose the one which yields optimal sensitivity. These criteria are general and can easily be applied to other methods not treated in this article.

Fast CSI protocols can be demanding on the available instrumentation, especially on gradient hardware or the receiver. As the performance of NMR instruments is continuously improving, fast CSI sequences should find widespread use in clinical and biomedical applications.

ACKNOWLEDGMENTS

This work was supported by the Deutsche Forschungsgemeinschaft, Ki 433/2-2 and Ki 433/5-1, and the French–German PROCOPE program.

REFERENCES

1. J. W. Hugg, K. D. Laxer, G. B. Matson, A. A. Maudsley, C. A. Husted, and M. W. Weiner, *Neurology* **42**, 2011–2018 (1992).
2. T. C. Ng, Y. G. Comair, M. Xue, N. So, A. Majors, H. Kolen, H. Luders, and M. Modic, *Radiology* **193**, 465–472 (1994).
3. J. Vion-Dury, S. Confort-Founy, F. Nicoli, C. Dhiver, J.-A. Gastaut, J.-L. Gastaut, and P. J. Cozzone, *C. R. Acad. Sci. Paris, Life Sci.* **317**, 833–840 (1994).
4. W. G. Negendank, *NMR Biomed.* **5**, 303–324 (1992).
5. P. A. Bottomley, *Radiology* **191**, 593–612 (1994).
6. G. M. Pohost, *Circulation* **92**, 9–10 (1995).
7. A. A. Maudsley, S. K. Hilal, W. H. Perman, and H. E. Simon, *J. Magn. Reson.* **51**, 147–152 (1983).
8. A. Ziegler, M. von Kienlin, Y. Le Fur, C. Rubin, M. Décorps, and C. Rémy, "13th Annual Meeting of the ESMRMB, 1996," p. 234.
9. A. Metzler, M. Izquierdo, A. Ziegler, W. Köckenberger, E. Komar, M. von Kienlin, A. Haase, and M. Décorps, *Proc. Natl. Acad. Sci. USA* **92**(25), 11912–11915 (1995).
10. R. R. Ernst and W. A. Anderson, *Rev. Sci. Instrum.* **37**, 93–101 (1966).
11. D. E. Jones and H. Sternlicht, *J. Magn. Reson.* **6**, 167–182 (1972).
12. D. I. Hoult and R. E. Richards, *J. Magn. Reson.* **24**, 71–85 (1976).
13. D. I. Hoult and P. C. Lauterbur, *J. Magn. Reson.* **34**, 425–433 (1979).
14. R. R. Ernst, G. Bodenhausen, and A. Wokaun, "Principles of Nuclear Magnetic Resonance in One and Two Dimensions," Oxford Univ. Press, Oxford (1987).
15. E. D. Becker, J. A. Ferretti, and P. N. Gambhir, *Anal. Chem.* **51**, 1413–1420 (1979).
16. G. Johnson and E. X. Wu, *J. Magn. Reson. B* **105**, 238–241 (1994).
17. P. T. Callaghan and C. D. Eccles, *J. Magn. Reson.* **71**, 426–445 (1987).
18. R. R. Ernst, *Adv. Magn. Reson.* **2**, 1–135 (1966).
19. G. C. McKinnon, *Magn. Reson. Med.* **30**, 609–616 (1993).
20. A. A. Maudsley, *J. Magn. Reson.* **68**, 363–366 (1986).
21. T. R. Brown, B. M. Kincaid, and K. Urgulbil, *Proc. Natl. Acad. Sci. USA* **79**, 3523–3526 (1982).
22. A. Haase, D. Leibfritz, and W. Werk, *Magn. Reson. Med.* **7**, 358–363 (1988).
23. D. B. Twieg, D. J. Meyerhoff, B. Hubesch, K. Roth, D. Sappey-Marinié, M. D. Boska, J. R. Gober, S. Schaefer, and M. W. Weiner, *Magn. Reson. Med.* **12**, 291–305 (1989).
24. J. H. Duyn and C. T. W. Moonen, *Magn. Reson. Med.* **30**, 409–414 (1993).
25. R. E. Sepponen, *Magn. Reson. Imaging* **3**, 163–167 (1985).
26. H. W. Park and Z. H. Cho, *Magn. Reson. Med.* **3**, 448–553 (1986).
27. W. T. Dixon, *Radiology* **153**, 189–194 (1984).
28. A. Haase, J. Frahm, D. Matthaei, K. D. Merboldt, and W. Hänicke, Abstracts of the Society of Magnetic Resonance in Medicine, 4th Annual Meeting, London, p. 980 (1985).
29. A. Haase, J. Frahm, D. Matthaei, K. D. Merboldt, and W. Hänicke, *J. Magn. Reson.* **67**, 258–266 (1987).
30. A. Haase and D. Matthaei, *J. Magn. Reson.* **71**, 550–553 (1987).

31. A. Haase, *Magn. Reson. Med.* **13**, 77–89 (1990).
32. P. Mansfield, *J. Phys. C* **10**, L50–L58 (1977).
33. M. Doyle and P. Mansfield, *Magn. Reson. Med.* **5**, 255–261 (1987).
34. P. Mansfield, *Magn. Reson. Med.* **1**, 370–386 (1984).
35. A. M. Cormack, *J. Appl. Phys.* **34**, 2722–2727 (1963).
36. P. C. Lauterbur, *Nature* **242**, 190–191 (1973).
37. E. Adalsteinsson, P. Irarrazabal, B. M. Spielman, and A. Macovski, *Magn. Reson. Med.* **33**, 461–466 (1995).
38. Guilfoyle *et al.*, *Magn. Reson. Med.* **10**, 282–287 (1989).
39. S. Posse, G. Tedeschi, R. Risinger, R. Ogg, and D. Le Bihan, *Magn. Reson. Med.* **33**, 34–40 (1995).
40. D. G. Norris, *Magn. Reson. Med.* **17**, 539–542 (1991).
41. J. Hennig, A. Nauwerth, and H. Friedburg, *Magn. Reson. Med.* **3**, 823–833 (1986).
42. J. Hennig, *J. Magn. Reson.* **78**, 379–407 (1988).
43. D. G. Norris and P. Börnert, *J. Magn. Reson. A* **105**, 123–127 (1993).
44. D. G. Norris, P. Börnert, T. Reese, and D. Leibfritz, *Magn. Reson. Med.* **27**, 142–157 (1992).
45. D. G. Norris and W. Dreher, *Magn. Reson. Med.* **30**, 641–645 (1993).
46. P. M. Jakob, M. Décorps, A. Ziegler, and S. Doran, *Magn. Reson. Med.* **33**, 573–578 (1995).
47. J. Hennig and M. Hodapp, *MAGMA* **1**, 39–48 (1993).
48. J.-J. Dunant and J. Delayre, U.S. Patent 3975675 (1976).
49. P. van Gelderen, J. H. Duyn, and C. Moonen, *J. Magn. Reson. B* **107**, 78–82 (1995).
50. D. N. Guilfoyle and P. Mansfield, *Magn. Reson. Med.* **2**, 479–489 (1985).
51. P. M. Jakob, F. Kober, R. Pohmann, and A. Haase, *J. Magn. Reson. B* **110**, 278–283 (1996).
52. D. B. Twieg, *Magn. Reson. Med.* **12**, 64–73 (1989).
53. A. Ziegler, C. Delon-Martin, R. Dupeyre, J. F. Peyridieu, A. Baudot, J. Mazuer, J. Odin, J. L. Descotes, E. Payen, O. Skowron, P. M. Jakob, and F. Kober, "SMR/ESMRMB Joint Meeting 1995," p. 1917.
54. M. L. Bernardo, P. C. Lauterbur, and L. K. Hedges, *J. Magn. Reson.* **61**, 168–174 (1985).
55. M. Meininger, P. M. Jakob, and M. von Kienlin, A. Haase, "SMR/ESMRMB Joint Meeting 1995," p. 1900.
56. H. R. Brooker, T. H. Mareci, and J. T. Mao, *Magn. Reson. Med.* **5**, 417–433 (1987).